Structural Engineering and Mechanics, *Vol. 57, No. 5 (2016) 951-968*
DOI: http://dx.doi.org/10.12989/sem.2016.57.5.951

Experimental investigation on a freestanding bridge tower under wind and wave loads

Xiaodong Bai[1], Anxin Guo[*1], Hao Liu[1], Wenli Chen[1], Gao Liu[2], Tianchen Liu[2], Shangyou Chen[2] and Hui Li[1]

[1]*Ministry-of-Education Key Laboratory of Structural Dynamic Behavior and Control, School of Civil Engineering, Harbin Institute of Technology, Harbin, China*
[2]*Bridge Technology Research Center, CCCC Highway Consultants Co., Ltd., Beijing, China*

(Received July 4, 2015, Revised January 28, 2016, Accepted January 29, 2016)

Abstract. Long-span cross-strait bridges extending into deep-sea waters are exposed to complex marine environments. During the construction stage, the flexible freestanding bridge towers are more vulnerable to environmental loads imposed by wind and wave loads. This paper presents an experimental investigation on the dynamic responses of a 389-m-high freestanding bridge tower model in a test facility with a wind tunnel and a wave flume. An elastic bridge model with a geometric scale of 1:150 was designed based on Froude similarity and was tested under wind-only, wave-only and wind-wave combined conditions. The dynamic responses obtained from the tests indicate that large deformation under resonant sea states could be a structural challenge. The dominant role of the wind loads and the wave loads change according to the sea states. The joint wind and wave loads have complex effects on the dynamic responses of the structure, depending on the approaching direction angle and the fluid-induced vibration mechanisms of the waves and wind.

Keywords: freestanding bridge tower; experimental investigation; wind and wave; offshore/coastal structures

1. Introduction

Cross-strait bridges are an important type of civil infrastructure for vehicle and railroad transportation across straits and gulfs. With rapid social and economic development in coastal areas, more cross-strait bridges have been constructed or are being planned around the world, especially in China. Cable-stayed bridges and suspension bridges with long spans are the main structural types that meet the functional requirements of ship navigation with both large clearances and widths in cross-strait transportation systems. For a long-span bridge with a long natural period proportional to its span (Diana *et al*. 2013), the structure is vulnerable to wind and wave loads. Furthermore, the construction of a long-span bridge is a long process. During the construction stages, the structures have not yet reached a completed status; therefore, the safety of the freestanding bridge towers is an important issue when sustaining severe wind and wave actions,

*Corresponding author, Professor, E-mail: guoanxin@hit.edu.cn

http://www.techno-press.org/?journal=sem&subpage=8 ISSN: 1225-4568 (Print), 1598-6217 (Online)

which occur during these stages.

Wind is a common load applied on the long-span bridges. The wind effects on the long-span bridge includes the fluid-induced vibration of bridge deck (Jain *et al*. 1996), cable (Xu and Wang 2003, Gu 2009, Chen *et al*. 2010) and tower (Belloli *et al*. 2011, Siringoringo and Fujino 2012). In the freestanding configuration, the wind-induced response of a self-supporting pylon includes buffeting and vortex-induced vibration (VIV). Based on health monitoring data, Siringoringo and Fujino (2012) indicated that the H-shaped tower of the Hakucho Suspension Bridge was dominated by buffeting responses in the along-wind direction while the cross-wind vibration of the structure included the VIV due to the interference of the two legs. The wind-induced vibration of the 367 m H-shaped tower of the Messina Bridge was also analyzed based on wind tunnel test results with a longitudinal turbulence of 12% (Larose *et al*. 1995). It was concluded that the vortex-induced vibration (VIV) dominated the aerodynamic responses. An in-situ measurement of the wind-induced responses of the 254 m freestanding bridge tower of the Storebæ lt East Bridge found that the in-line tandem arrangement of the two legs induced a considerable VIV response (Larose *et al*. 1998). Ricciardelli (1996) proposed a semi-empirical method to analyze and predict the wind-induced responses of the flexural bridge tower based on the framework of the linearized quasi-steady theory. Belloli *et al.* (2011) experimentally investigated the aerodynamic characteristics of a cable-stayed bridge tower in freestanding configuration. A 1:30 scaled sectional model and a 1:100 scaled full aeroelastic model of the bridge tower were used in this study and the scale effects in wind tunnel testing are analyzed.

For bridges in marine environments, the natural periods of both the freestanding bridge towers and the completed whole bridges might fall in the energy band of the ocean waves, which are approximately 3-25 s in terms of the wave period (Chakrabarti 2005). Therefore, aside from the wind loading, the wave loads also pose a challenge for long-span coastal bridges. Unfortunately, there has been little research reporting the structural behavior of bridge towers in wind-wave environments. Only the dynamic responses of a floating bridge subjected to wind and waves separately has been investigated in Osaka by Watanabe *et al*. (2000). However, in the research fields of offshore platform and wind turbines, dynamic responses and structural safety under wind-wave conditions have received considerable attention from researchers and engineers. Some related studies on this topic are introduced in the follows to shed light on the current study.

For articulated loading platforms (ALPs) that typically have slender vertical columns, an experiment conducted by Daneshvaran and Vickery (1995) indicated that large waves can significantly reduce the structural resonant responses induced by fluctuant wind. This finding was confirmed by other researchers studying a double-hinged articulated tower (Zaheer and Islam 2008, 2012). It was concluded that when the wave frequency was close to the fundamental frequency, the wind contribution was insignificant and suppressed by waves; while when the wave frequency was away from the resonant frequency, the wind played a dominant role. Tension-leg platforms (TLPs) are also vulnerable to wind excitation, especially for surge motion (Kareem 1983). The experimental work of Vickery (1995) also showed a similar result to that of the ALPs (Daneshvaran and Vickery 1995).

As an important part of renewable energy exploitation, offshore wind turbines have also received increasing attention in the context of structural safety under wind-wave conditions (Breton and Moe 2009). Manenti and Petrini (2010) conducted a frequency domain analysis on a fixed offshore wind turbine using the commercial software ANSYS, and the results indicated that the dynamic responses of the structures under wind-wave combining action were less than the sum of the separate results of wind-only and wave-only conditions. Floating offshore wind turbines

(FOWT) are more attractive with respect to higher production in the open sea but similarly face a complex marine environment. Recently, various numerical methods considering wind-wave loads have been developed for FOWTs (Jonkman 2007, Jensen *et al*. 2011, Philippe *et al*. 2013, Utsunomiya *et al*. 2014).

This paper presents an experimental study on the dynamic responses of a freestanding bridge tower that is located at an intermediate water depth of approximately 47 m and is subjected to multiple wind and wave actions. An elastic model with a geometric scale of 1:150 was experimentally used in a wind tunnel and wave flume test facility. This paper is organized into three parts. First, the details of the prototype tower, the sea state and the test facility are introduced. Second, the experimental program, including the test model, the measurement system and the test plan, is presented. Third, the experimental results are analyzed and discussed. The dynamic responses of the structure under wind load have previously been analyzed. Therefore, the wave-induced vibration and dynamic responses under wind-wave actions are investigated to determine the effects of the oscillation mechanism of the structure under complex environmental loads. The experimental results indicate that the joint action of the wind and waves exhibits complex effects on the structural dynamic responses due to the differences between the two frequency components and the fluid-induced vibration mechanisms of the waves and wind.

2. Prototype structure and the test facility

2.1 Prototype structure

The navigable bridge investigated in this study is a main component in the planned highway channel across the Qiongzhou Strait to connect Hainan Island and the Leizhou Peninsula in China. To accommodate the navigational requirements of large vessels, the span of the bridge is planned to exceed 1500 m, and the height of the concrete bridge tower reaches 388.9 m, as measured from the top of the foundation. Fig. 1 shows the configuration and the dimensions of the prototype structure with the bridge tower designed as a modified diamond-shaped concrete structure. The cross section of the tower legs is a hollow, approximately rectangular shape that varies linearly from the bottom to the cross beam at an elevation of 73.9 m and then maintains a dimension of 17.3 m×9.4 m above that area. On the top, an inverted V-shaped block is constructed to support the cables.

The pylon is located at a water depth of 46.6 m. A composite caisson-piles foundation consisting of a caisson and grouped piles, shown in Fig. 1(c), supports the upper structure and improves its capacity to resist external loads. This caisson foundation has an approximately elliptic section combining a central rectangle of 63 m×20 m and two external half circles with diameters of 63 m. The caisson foundation is at 93.3 m depth with an embedment depth of 40.0 m in the soil. Through finite element analysis it has been determined that the bridge tower in a freestanding configuration has a natural period of 9.71 s and 4.48 s for the first flexural modes along the *y*- and *x*-directions, respectively, and of 1.86 s for the first torsional mode.

2.2 Sea state

According to the meteorological and hydrological data, extreme sea states with return periods of 25 and 100 years were provided for the laboratory test (Table 1). For the sea states with 25-year

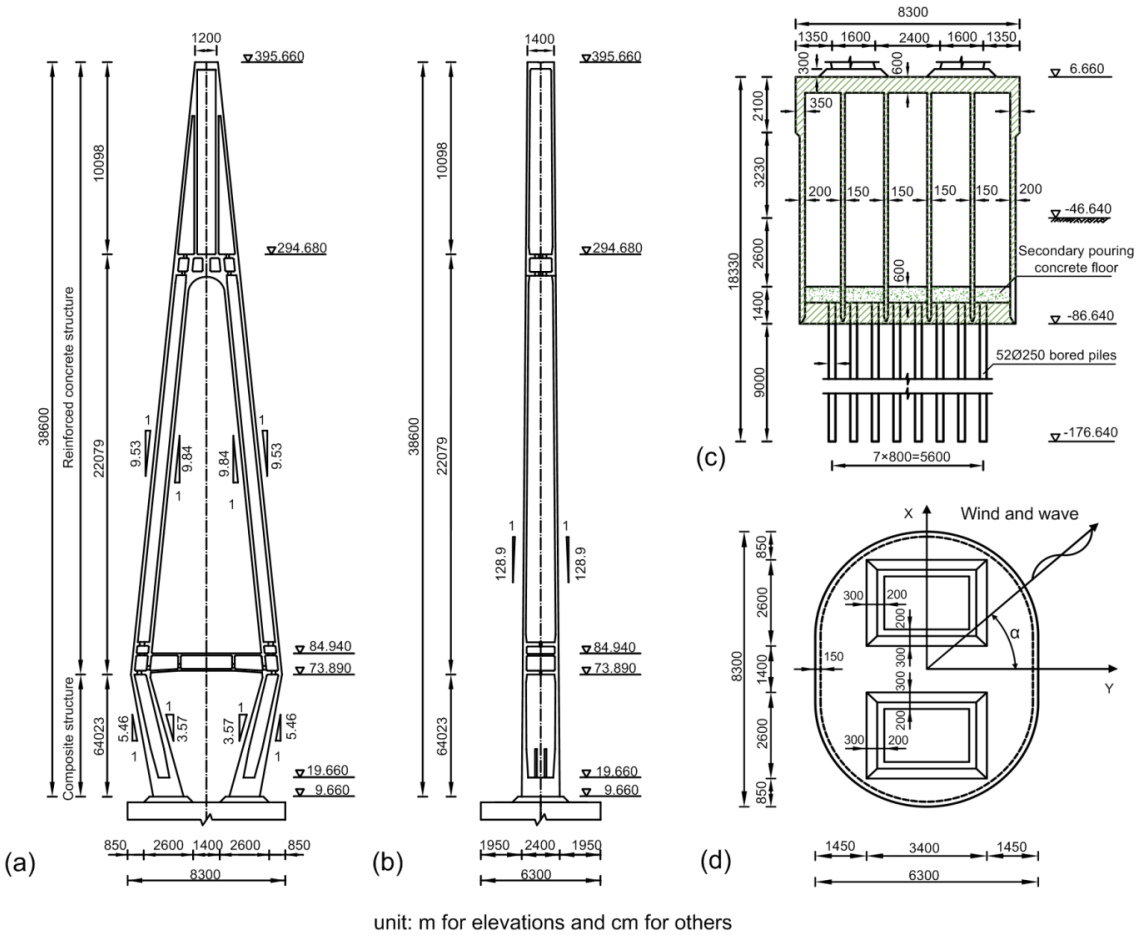

Fig. 1 Schematic of the freestanding bridge tower: (a) front view, (b) lateral view, (c) elevation of the foundation and (d) cross section of the foundation

Table 1 Extreme sea states of the wind and waves; the scaled parameters for the model tests

Return period (year)	Loading Case	Wind		Wave	
		V_{10} (m/s)	γ	$H_{1/3}$ (m)	$T_{1/3}$ (s)
25	wind only	45.4/3.71	0.12	—	—
	wave only	—	—	7.1 /0.047	8.7/0.71
	wind and wave	45.4/3.71	0.12	7.1/0.047	8.7/0.71
100	wind only	51.6/4.21	0.12	—	—
	wave only	—	—	8.6/0.057	9.6/0.78
	wind and wave	49.0/4.00	0.12	8.6/0.057	9.6/0.78

Note: The values after the slash are the scaled parameters for model tests.

and 100-year return periods, the design mean speeds at a 10 m elevation, V_{10}, were obtained as 45.4 and 51.6 m/s, respectively. The mean wind speed profile was assumed to match the open sea

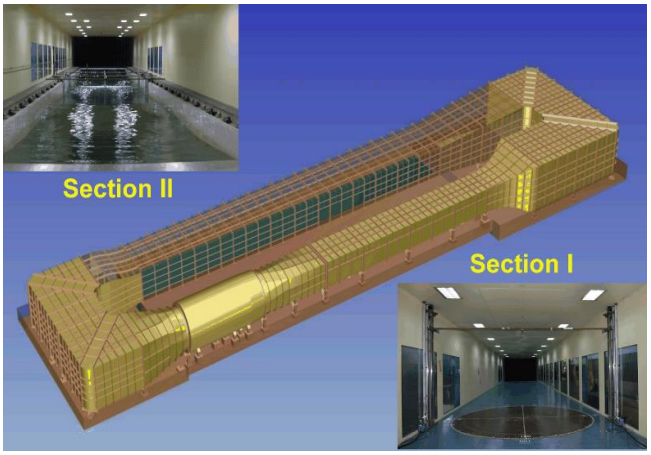

Fig. 2 Test facility with the wind tunnel and wave flume

terrain with an exponent of 0.12. The corresponding significant wave height, $H_{1/3}$, and wave period, $T_{1/3}$, were determined to be 7.1 m and 8.7 s and 8.6 m and 9.6 s, respectively. For the wind-wave actions, the mean wind speed, significant wave height and wave period were proposed based on the wind and wave in-situ measurement data and are listed in Table 1.

2.3 Test facility

The experiments were conducted in the Wind Tunnel and Wave Flume Laboratory at the Harbin Institute of Technology in China. The test facility used in this study uses a novel equipment integrating two wind tunnel test sections and a wave flume, as illustrated in Fig. 2. The facility is 89 m long and 21 m wide. Section I is a common wind tunnel with dimensions of 4.0 m×3.0 m×25.0 m, and the wind speed can be adjusted from 3.0 m/s to 44.0 m/s. On the other side, the test section consists of a large wind tunnel with dimension of 5.0 m×4.5 m×50 m and a wave flume with dimension of 6.0 m×3.6 m×50 m.

The wave flume can be covered by moveable floors that are driven by a series of electric motors. In this configuration, the facility serves as a conventional wind tunnel to conduct wind tunnel tests in both sections. With the removal of the floors, hydrodynamic experiments or coupling tests under wind and wave conditions can be performed. In the wave flume, a bottom-hinged flap-type wavemaker is installed to generate water waves while a wave absorber is equipped at the opposite side to dissipate the wave energy. A 5.0 m×9.0 m lift platform is equipped above a deep well. During the experiment, the test model was mounted on the platform and then adjusted to the required submergence depth by driving the mechanical devices of the platform.

3. Experimental setup

3.1 Test model

For model designs of structures under wave loads, the Froude number is the primary non-dimensional parameter that needs to be satisfied. However, the Reynolds number is another

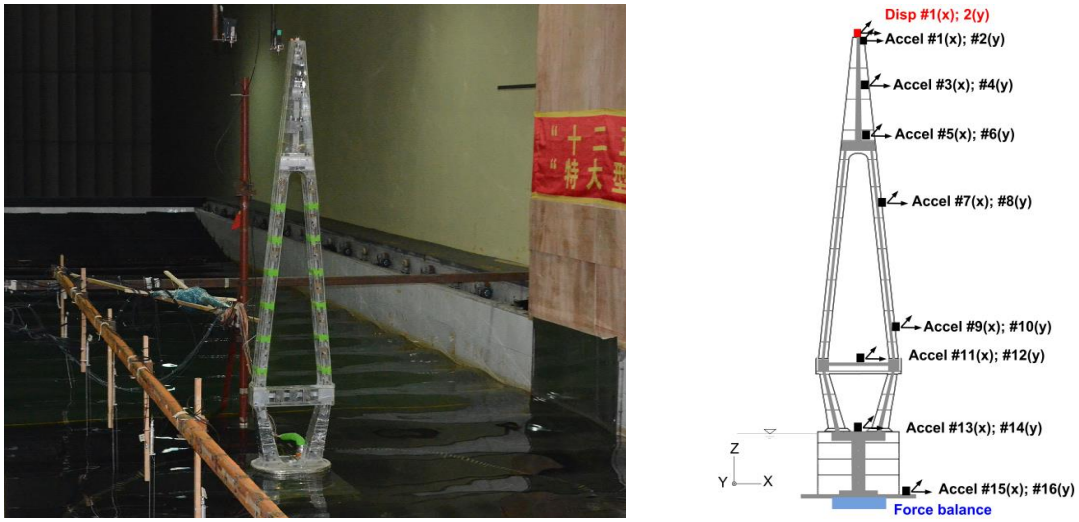

(a) Photograph of the model installed in the testing facility (b) The locations of the sensors

Fig. 3 The test model

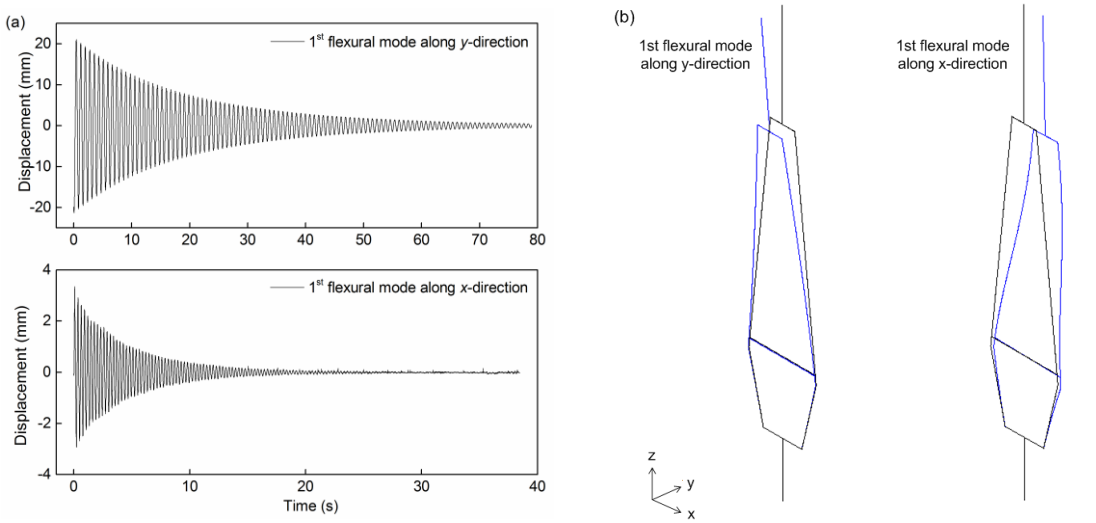

(a) Free vibration test results (b) The mode shapes

Fig. 4 Dynamic characteristics of the test model

important non-dimensional parameter that affects the wind-induced vibration of structures. Theoretically, the Froude and Reynolds similitude criterion should be simultaneously considered for the model test of a structure under wind and wave actions. However, both parameters cannot be satisfied simultaneously in a laboratory test. The Froude similarity law was employed for the test model design. In this study, the Reynolds number of the prototype structure and test model were calculated to be 6.3×10^7 and 3.4×10^4, respectively. The Reynolds number discrepancy ($10^{6\sim7}$ of prototype to $10^{4\sim5}$ of test model) generally yields conservative designs for structures with simple circular sections (Sumer and Fredsøe 1997) and rectangular sections (Holmes 2001). Therefore,

the effects of this factor were not considered in the current experimental work.

The test model of the bridge tower was designed and manufactured based on the Froude similarity criterion. As shown in Fig. 3(a), the test model consisted primarily of an internal aluminum spine and external perspex covers. The aluminum spine was designed according to the stiffness of the actual structure and its corresponding scaling to represent the elastic properties of the bridge tower. The external covers, which were attached on the internal spine, were manufactured in accordance with the dimensions of the structure to satisfy the aerodynamic shape. Along the height of the tower, the tower model was divided into 18 sections with a 1-2-mm gap between neighboring sections. Thin films were used to prevent air and water movement between the modulus gaps. The inertial properties of the structure were matched by attaching additional lump mass to the aluminum spine. After installing the bridge model in the platform, the mode characteristics of the tower model were tested under conditions without water. Fig. 4(a) shows the displacement responses at the top of the tower in the *x*- and *y*-directions. Based on the test results, the first two natural periods and damping ratios of the test model were found to be 0.786 s and 0.71%, 0.282 s and 0.93%, for the 1st flexural mode in the *y*- and *x*-directions, respectively. The mode shapes of the test model are shown in Fig. 4(b).

3.2 Measurement instrument

High frequency base balance, accelerometer and displacement transducers were included on the test model to measure the dynamic responses of the structure. During the tests, 16 accelerometers were mounted inside the model to measure the vibration of the bridge tower, as shown in Fig. 3(b). The reason for including so many accelerometers was to test the mode shapes and to validate the test model. Among them, 12 single-axes B&K 4507B accelerometers, which were divided into six groups, were used to independently measure the acceleration signals in the *x*- and *y*-directions. Furthermore, four Kyowa ASW-2A waterproof accelerometers were included in the bottom region to measure the acceleration response of the foundation in the two orthogonal directions. Two Keyence LK-G405 laser displacement transducers were installed on the top of the bridge tower to measure the horizontal displacement responses along the two axes of the structure. A force balance was installed at the base of the structure to measure the shear forces and the bending moments of the structure.

For the water wave, five capacitance-type wave gauges were installed along the wave flume to measure the wave surface elevations near the test model, as shown in Fig. 3(a). For the wind field, the wind speed profile and turbulence intensity were obtained using a Setra 239 micro differential pressure transducer. During the tests, the analog test signals were synchronously collected using a NI PXI-based data acquisition system. A sampling frequency of 1000 Hz and an analog low-pass filter at 100 Hz were employed to record the structural responses.

3.3 Test plan

Three types of experiments were performed including a hydrodynamic experiment with water waves, an aeroelastic experiment with wind loads, and an experiment with joint wind and wave loads. The first experiment measured the dynamic responses of the structure to wave forces applied by regular waves. According to the hydrogeological conditions, a significant wave period with a return period of 100 years is 9.6 s, which approaches the first natural period of 9.71 s of the structure in the *y*-direction. Under such a sea state, large resonant responses could possibly occur

when the freestanding structure is subjected to wave loads. As the resonant phenomenon poses a great challenge to the preliminary design, it is investigated in this study.

The aeroelastic experiment focused on the responses of the structure under wind loads. In this stage, although some small-amplitude waves were generated by the wind flowing on the liquid-vapor interface, the wind-generated wave in the facility was actually small compared to the design wave conditions, and the significant wave periods were also far from the structural period. Therefore, the effects of the wind-generated waves were negligible in this study, and the structure was regarded as being sustained by only the wind action. For the test case with wind and wave loads, the scaled values of the flow properties are listed in Table 1.

During the test, the effects of the directional angle of the fluid were also examined. For the convenience of the following analysis, the angle between the incident direction of the fluid and the *y*-direction of the structure, which was rotated together with the test model, is defined as the direction angle. Based on the above definition, the dynamic responses of the structural model were measured with a direction angle of 0-90° and with an increment of 22.5°. For a specific sea state, the same statistical properties of the wind and wave were used for all of the directional angles of the fluid actions.

4. Test results

4.1 Flow test with wind and waves

The flow field characteristics of the wind tunnel were calibrated before the model test. To match the mean wind speed profile, seven spires were installed at the entrance of the incoming flow. Moreover, because there was an elevation difference of approximately 1.0 m between the bottom of the wind tunnel and the still water level, a downstream ramp with a slope of 1/6 was included to improve the flow quality, as shown in Fig. 5. Furthermore, two windward standing walls were placed on both sides of the test platform, as illustrated on the right side of Fig. 3a, to eliminate the effects of the width difference of the wind tunnel and the wave flume that could lead to a distortion of the mean wind speed profile.

Fig. 6 shows the mean wind speed profile and the turbulence intensity of the test section. Because the motion of the wind generates small-amplitude waves and sprays at the surface of the

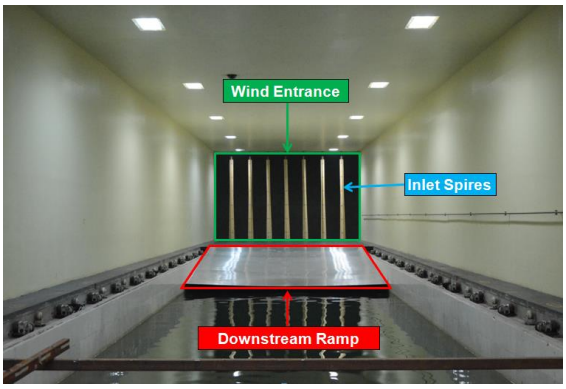

Fig. 5 Inlet spires and the downstream ramp

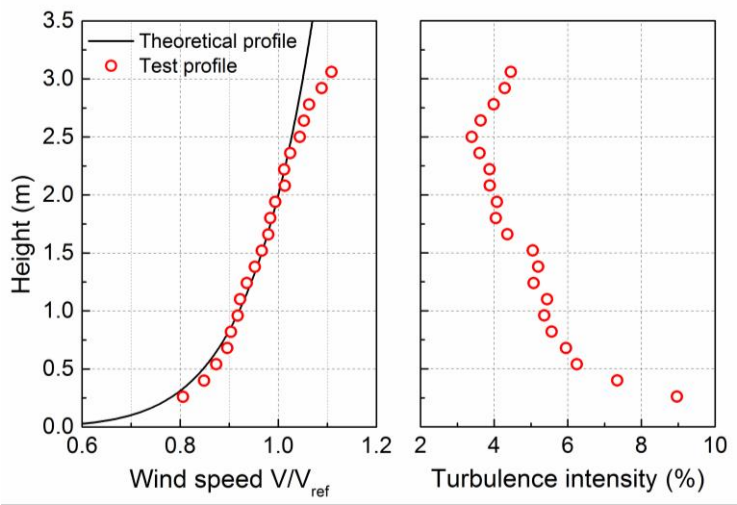

Fig. 6 Mean wind velocity profile and turbulence intensity

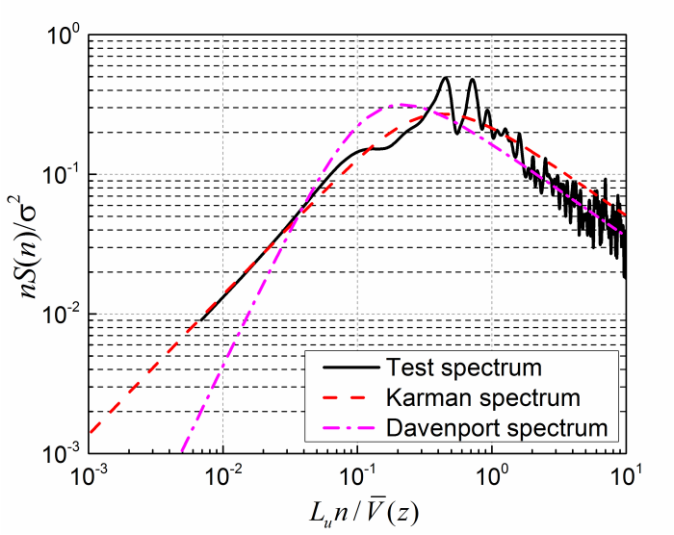

Fig. 7 Power spectra of the wind speed

water, only wind speeds above 0.25 m of the still water level were measured to maintain the safety of the sensor. Fig. 6 indicates that the wind speed profile matched the sea terrain with a power index of 0.12. The turbulence intensity was within the range of 3% to 10%. Fig. 7 shows the power spectra of the fluctuating wind from the measured data together with the simulated Davenport and Karman spectrums. It can be seen that the test data has a satisfactory agreement with the Karman spectrum.

For the water waves, regular waves corresponding to the given significant wave height and wave period of the sea states were generated using the wavemaker. Before the tests, the generated waves were calibrated using the feedback signals of the wave gauges to obtain the target waves in the wave flume without the test model installed.

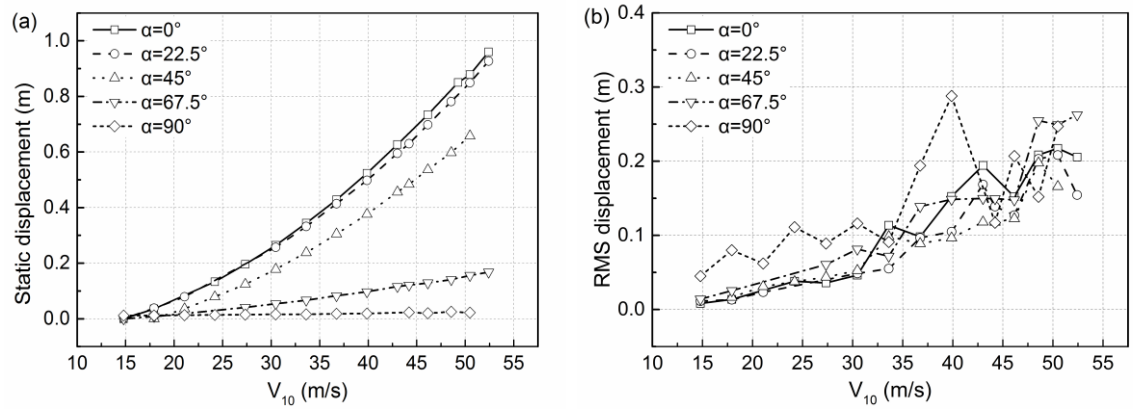

(a) The static displacement (b) The RMS displacement

Fig. 8 Displacement of the structure in the *y*-direction versus the mean wind speed

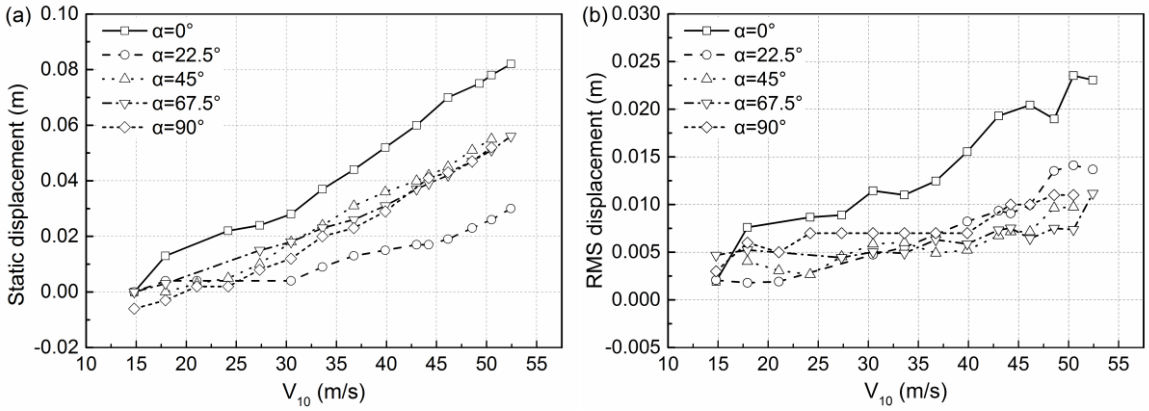

(a) The static displacement (b) The RMS displacement

Fig. 9 Displacement of the structure in the *x*-direction versus the mean wind speed

4.2 Dynamic responses of the structure under wind loads

The tower model was initially tested under just wind action in the test facility with the mean wind velocity, V_{10}, increasing from 14.8 m/s to 52.4 m/s for the prototype structure. In the following analysis, the test results are all scaled to that of the prototype structure according to the similarity law. Furthermore, it is considered that the responses of the structure are primarily dominated by the first two structural modes in the two directions, and the maximum displacement and acceleration responses occur at the top of the tower under the wind and wave loads. Therefore, only the top displacement and acceleration responses are analyzed in this article due to space limitations.

Based on the test results of the laser displacement transducer, the mean and root mean square (RMS) displacement responses at the top of the structure are shown in Figs. 8-9, respectively, for the two corresponding directions versus the increasing mean wind speed. It can be observed that the static deflection of the tower in the *y*-direction gradually increased with increasing wind speed,

and the maximum value was up to 0.96 m for a direction angle of 0°. It is also observed that the wind-induced vibration of the structure was primarily dominated by the buffeting loads. Furthermore, the crosswind static and RMS displacements in the *x*-direction were very small, approximately 1/10 of those in the *y*-direction.

The effects of the wind direction angle are also revealed in these figures. The static-displacement in the *y*-direction dropped significantly when the wind direction angle shifted from 45° to 67.5°. When the wind direction angle changed to 90°, a typical vortex induced vibration was measured in the velocity range of 32.5 to 45 m/s. Within this range, the vortex shedding frequency approached the natural frequency of the structure and resonant responses tended to develop. As a result, the vortex shedding frequency is captured by the natural frequency of the structure and the displacement in the *y*-direction was substantially larger than that of the conventional buffeting responses at lower wind velocities. The RMS value of the measured displacement reached its peak (approximately 0.29 m) at a mean wind speed of 39.8 m/s. As the wind velocity continued to increase, the RMS displacement experienced a sudden decline. When the wind velocity exceeded the upper boundary of the lock-in range, the RMS displacement tended to increase again.

The aerodynamic force of the structure can be expressed in terms of the following non-dimensional form

$$C_{Fi} = \frac{F_i}{0.5\rho V_H^2 A_s} \tag{1}$$

where F_i is the shear force in the *x*- and *y*-directions; V_H is the mean wind speed at height H; A_s is the projected area of the structure perpendicular to the mean wind direction; and ρ is the air density. According to the measurement of the force balance, the mean force coefficients along the *x*- and *y*-directions of the structure are calculated and given in Fig. 10 as a function of the approaching wind direction. As shown in Fig. 10, the maximum mean force coefficient is approximately 1.2, and its values vary in an inverse tendency for the two different directions. The mean force coefficient along the *y*-axis of the structure varies more drastically within the range of 45-90°. The same phenomenon can also be found for the mean force coefficient along the *x*-direction within the range of 0-45°.

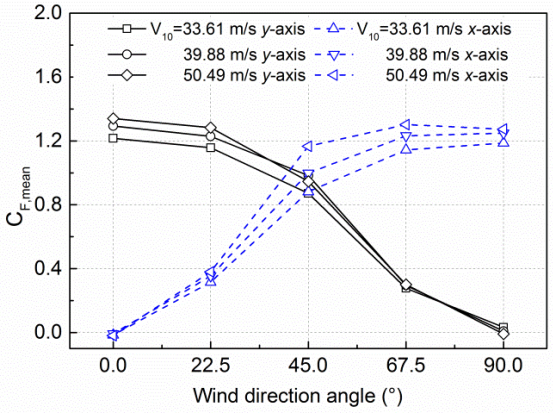

Fig. 10 Mean force coefficient versus the approaching wind direction

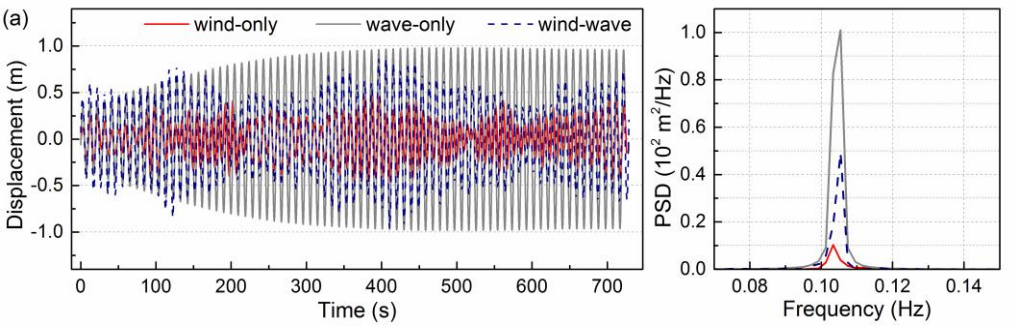

(a) The displacement

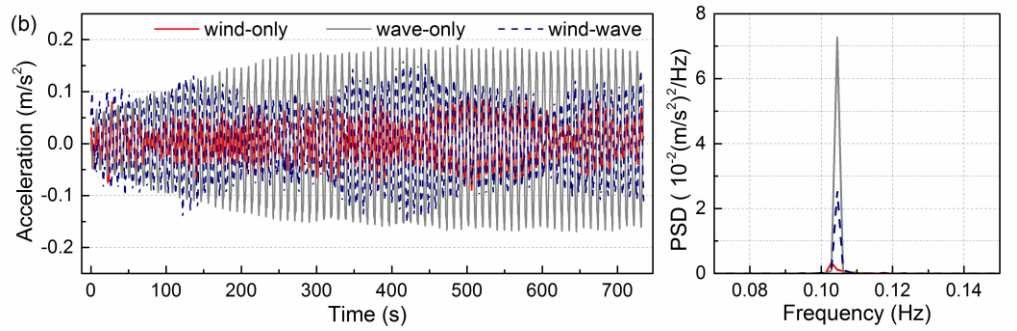

(b) The acceleration

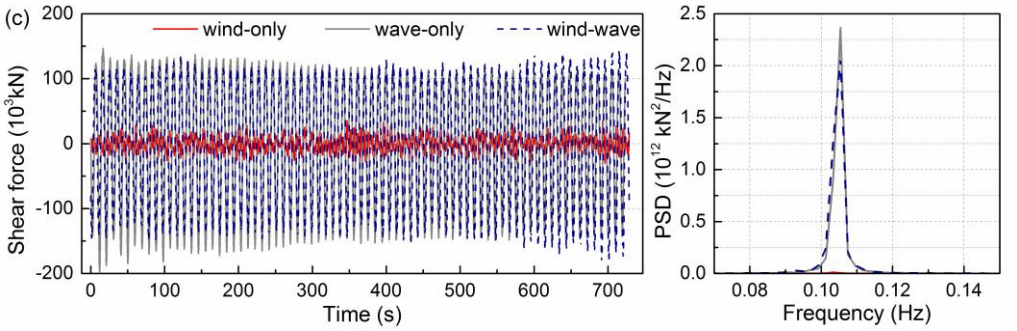

(c) The base shear

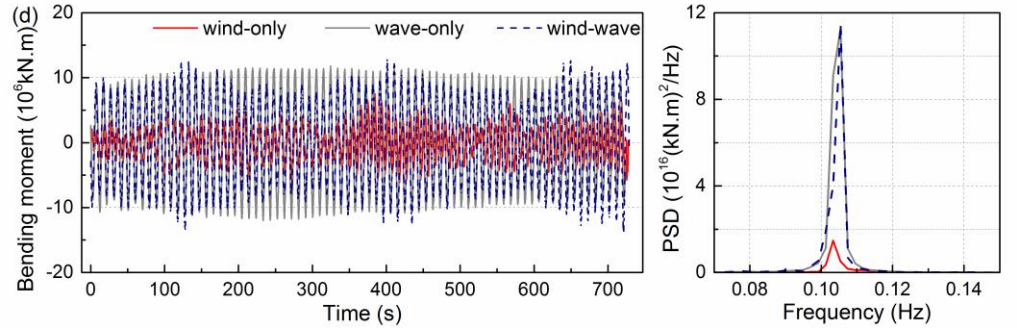

(d) The bending moment

Fig. 11 Time histories and spectra of the structural responses for an approaching directional angle of 0° with the 100-year return period of wind and waves

4.3 Dynamic responses of the structure under wind and wave loads

The dynamic responses of the test model under wind-only and wave-only loads are simultaneously analyzed in this section. In the wave-only tests, regular waves were generated on the bridge model by the wavemaker with significant wave periods of 0.71 and 0.78 s, corresponding to wave periods of 8.7 and 9.6 s, respectively, for the prototype structure. Under regular wave action, the structure harmonically oscillated. Fig. 11 shows the time history of the top displacement and acceleration, the base shear and the bending moment, M_x, of the structural model in the *y*-direction under wave loads with a 100-year return period and a directional angle of 0°. It is clear that the tip displacement undergoes a typically resonant vibration mode with gradually increasing amplitude until a steady amplitude of approximately 1.0 m is reached. This phenomenon is understandable because a wave period of 9.6 s is close to the natural period of the structure's 1st flexural mode in the *y*-direction. It should be noted that the drift ratio, defined as the top displacement versus the tower height, reaches 1/370, which poses an extremely dangerous condition for the tower from an engineering point of view. In this case, the maximum tip acceleration, the base shear force and the bending moment were found to be approximately 0.18 m/s^2, 100×10^3 kN and 10×10^6 kN.m, respectively.

For comparison, the time histories of the structural responses in cases of wind-only and wind-wave actions are also depicted in Fig. 11 with the same incident angle and return period. For comparison purposes, the structural responses induced by the mean wind loads are not included in this figure. The displacement and acceleration responses induced by the wind fluctuations were smaller than the resonant oscillation induced by the water waves. With the combined actions of the wind and waves, the top displacement was weakened compared to the wave-only test due to the superposition of the wind-induced fluctuation on the resonant oscillation by the wave. For the base shear, the wind-induced responses were significantly smaller than the wave responses. Therefore, the amplitude of the base shear in the wind-wave condition was quite close to the wave-only result. For the base bending moment, the wind effect was more significant than the base shear force because of the large moment arm of the wind load compared to the wave load.

The corresponding spectra of the structural responses are also given on the right side of Fig. 11. The dominant frequency of the dynamic responses with the wave load was identical to the wave period due to the forced vibration of the external loads on the foundation. However, the dominant frequency was shifted towards the natural frequency of the structure. Therefore, the superposition of the two different frequency components of the joint action of the wind and waves reduced the structural responses.

Fig. 12 compares the structural dynamic responses for different wind and wave actions for the 25-year return period with an incidence angle of 0°. The displacement response of the wind-only case was slightly smaller than that of the 100-year return period. For the wave load, the top displacement was significantly smaller than that of the 100-year return period because the wave period was not in the resonance region of the tower. The RMS value was approximately 1/14 of the resonance responses. It is also observed that the displacement responses were reduced with wind-wave action compared to wave-only tests. The corresponding RMS values for the 25-year return period were 0.144 m. For the base shear force, the wave force also plays a dominant role in this sea state. The displacement spectrum clearly shows that the wind-induced vibration was dominant for the 25-year return period with the frequency of the 1st flexural mode of the tower itself, while the wave-induced vibration was minor, with the wave period away from the structural resonance region. The wind effect on the base bending moment was comparable to the wave effect

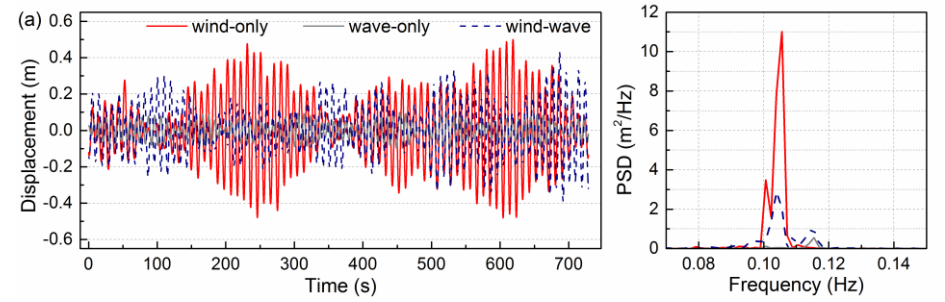

(a) The displacement

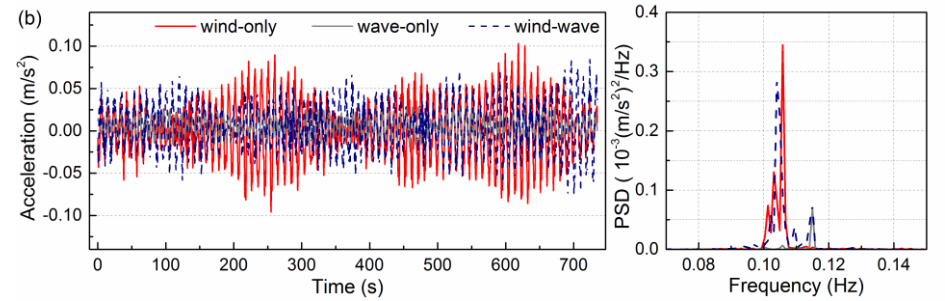

(b) The acceleration

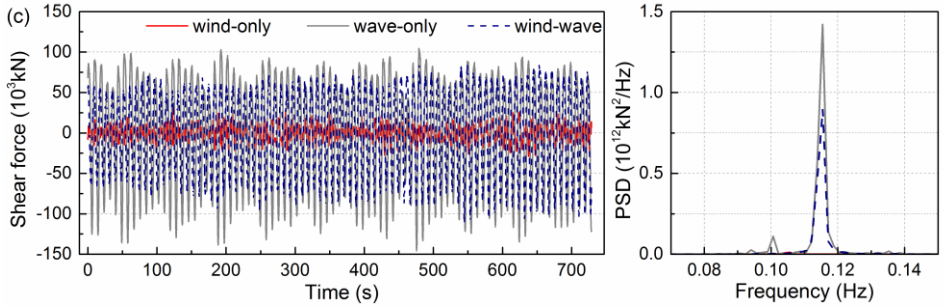

(c) The base shear

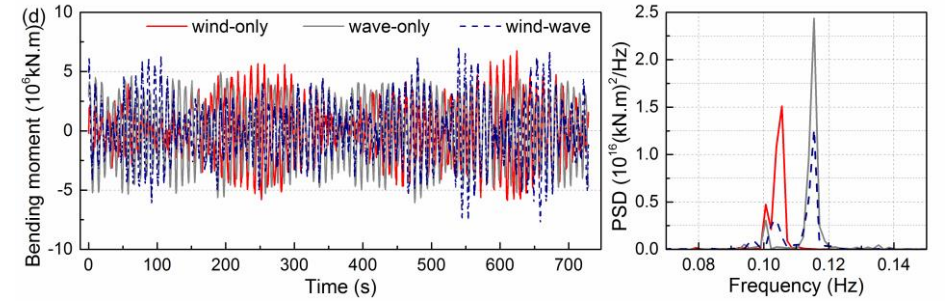

(d) The bending moment

Fig. 12 Time histories and spectra of the structural responses for an approaching direction angle of 0° with the 25-year return period of wind and waves

with two distinct frequencies, which is different from that of the 100-year return period because the resonant vibration was included. In that case, the bending moment was primarily induced by

the inertia force of the structure due to the resonant vibration under wave loads. Under the sea state of 25-year return period, the resonant vibration disappeared. Although the wind load was relative small compared to the wave load, the large arm induced a comparable bending moment in this test case.

The effects of combined wind and waves on the dynamic responses of the structure are revealed by the RMS values of the displacement in the *x*- and *y*-directions considering the effects of the directional angles for the sea states of the 25- and 100-year return periods. Fig. 13 shows the RMS values of the top displacement versus the directional angle of the fluid. It is clear that the *x*-direction displacement responses were very small for the three load cases because of the large stiffness of the bridge tower in the *x*-direction. For the 25-year return period, the *y*-direction RMS displacement variation versus the direction angle of wind and wave actions was not significant for the structure under the wave load. This is because the wave period of this sea state was not in the resonant region of the 1st flexural mode of the structure. However, the displacement responses of the 100-year return period increased nearly 13 times for an incident wave angle of 0°. Furthermore, the RMS displacement decreased with increasing incident angle because of projection area reduction and inertia coefficient variation with the rotation of the foundation.

The RMS displacement in the *y*-direction shown in Fig. 13 under wind and wave-coupling actions was smaller than a simple superposition of the displacement responses of the wind-only and wave-only states for wind and wave direction angles of 0°. However, for a direction angle of 45°, the displacement of the wind-wave action coincided with that of the wind-only case. Here, the contribution of the wave action was very small. Nevertheless, the dynamic displacement responses of the wind and wave coupling action were larger than that of the individual wind and wave loads for several directional angles. From the above analysis, it is clear that the displacement responses of the bridge tower strongly depend on the directional angle of the flows.

Fig. 14 shows the RMS values of the shear force on the foundation base. It is evident that the base shear was primarily caused by the water waves, and the wind-induced response was small. This is due to the large dimensions of the foundation and the inertia wave force according to MacCamy-Fuchs diffraction theory (McCormick 2009). The wave force presents an inverse tendency for the two different directions in the non-resonant cases of the 25-year return period. The base shear force in the *y*-direction declines as the incidence angle increases, while the inverse

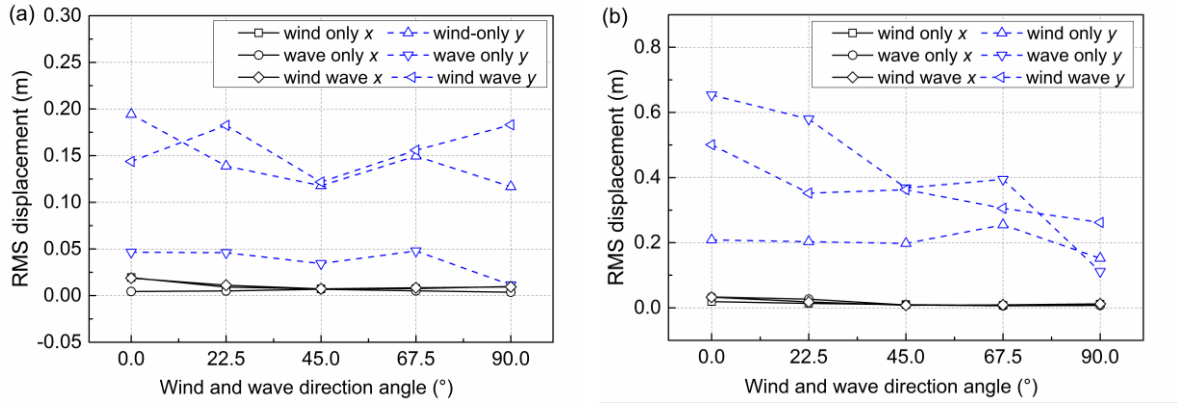

(a) 25-year return period (b) 100-year return period

Fig. 13 RMS values of the top displacement

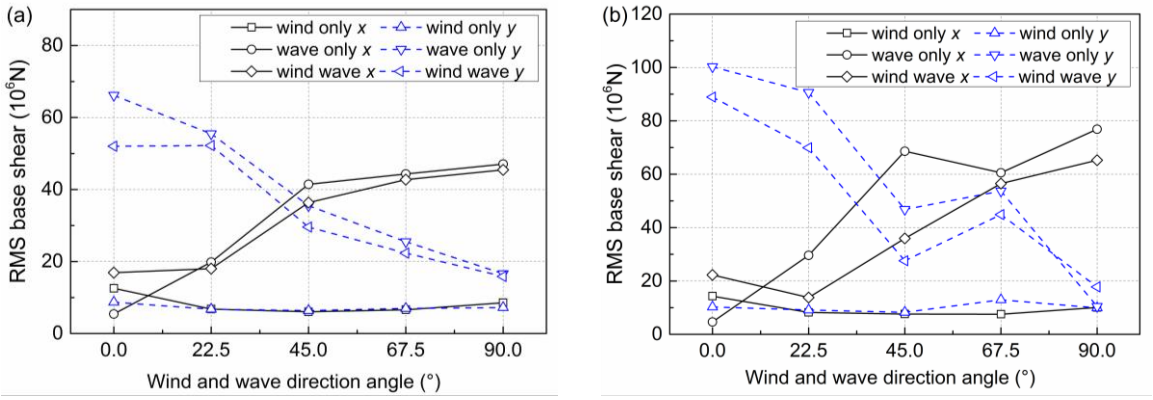

(a) 25-year return period (b) 100-year return period

Fig. 14 RMS values of the base shear force

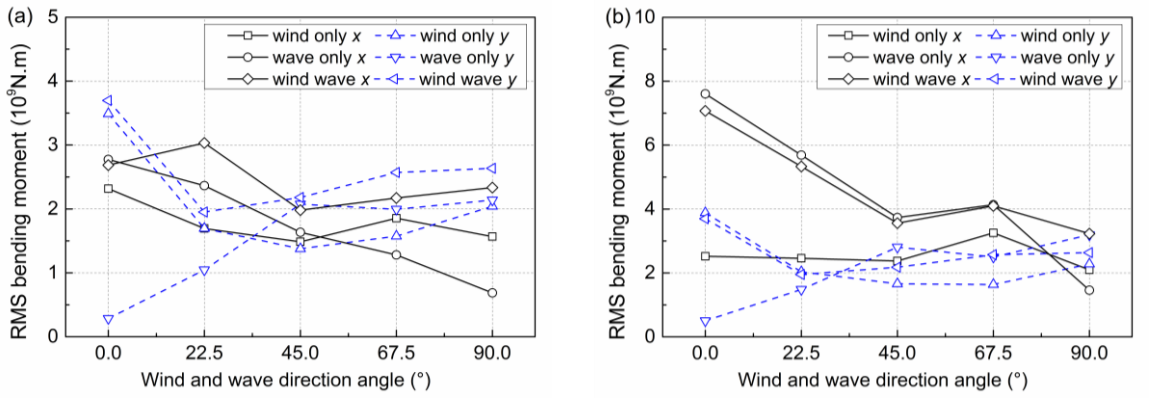

(a) 25-year return period (b) 100-year return period

Fig. 15 RMS values of the base bending moment

occurs in the *x*-direction. This phenomenon conforms to the specific configuration of the foundation (an unequal width of the two horizontal principal axes) and the decrease of the wave action projection area with an increase in the wave incident direction. The variation of the incident angle leads to an intersection of the *x*-component and *y*-component shear forces at approximately α=45°. The maximum RMS values of the base shear were found to be 47.1×10^3 kN at α=90° for the *x*-direction and 66.2×10^3 kN at α=0° for the *y*-direction with a ratio of 0.71, which is close to the width ratio of the foundation (63 m/83 m=0.76). The base shear forces exhibit a similar tendency with an increase in the direction angle of the fluid for the wave-only and wind-wave tests. Furthermore, the base shear force induced by the wind-wave loads was smaller than the sum of the wind-only and wave-only test results, even for the wave force. By contrast, the test results of the base shear under the 100-year return period were complicated due to resonant effects. It can be observed from Fig. 14 that the structural responses show a similar trend for the wave only and wind-wave test cases with the 25-year return period. However, for an incident angle of 45°, the structural responses were relatively small.

In Fig. 15, the RMS values of the base bending moment of the structure are plotted. It can be

observed that the wind load induced a comparable bending moment due to the large arm. Therefore, the values of the bending moment at the foundation base were of the same order and exhibited a similar tendency as the base shear force under the wind-only, wave-only and wind-wave conditions.

5. Conclusions

This paper presents an experiment on the dynamic responses of a freestanding bridge tower model under sea states with wind and wave action. A 1:150 elastic model was manufactured for the model test. The dynamic responses, including the displacement, acceleration, base shear and moment, were measured for the structural model under wind-only, wave-only, and wind-wave combined actions. From the measurement of the test signals, the dynamic responses were investigated to reveal the effects of the joint actions of the wind and waves. The concluding remarks of this study are as follows:

- When the wave period approaches the natural frequency of the structure, the resonant effects are important for the safety of the freestanding bridge tower.
- Joint wind and wave actions are complicated for a bridge tower. For the displacement, the structural responses under wind-wave loads are smaller than that under wind loads for a directional angle of 0° while the opposite is true for 90°. The effects of joint wind and wave action are dependent on the directional angle of the loads compared with the individual load action of the wind and waves.
- The base shear force of the bridge tower is mainly caused by water waves. Under the sea state, including the wind and wave loads, the wind reduced the base shear force induced by the water wave. Therefore, the base shear force with both wind and waves is smaller than just the wave force because of the different dominant vibration frequencies of the two loads. Due to the large moment arm, the wind load is the main factor contributing to the base bending moment of the structure.

Acknowledgments

The financial support provided by the Technology Project of the Ministry of Transport of China (2011318494150), the National Natural Science Foundation of China (51222808), the Fundamental Research Funds for the Central Universities of China (HIT.BRETIV.201320), and the Research Fund for the Doctoral Program of Higher Education of China (20122302110057) is greatly appreciated by the authors.

References

Belloli, M., Fossati, F., Giappino, S., Muggiasca, S. and Villani, M. (2011), "On the aerodynamic and aeroelastic response of a bridge tower", *J. Wind Eng. Ind. Aerod*., **99**(6-7), 729-733.

Breton, S. and Moe, G. (2009), "Status, plans and technologies for offshore wind turbines in Europe and North America", *Renew. Energy*, **34**(3), 646-654.

Chakrabarti, S. (2005), *Handbook of Offshore Engineering*, Elsevier, Oxford, UK.

Chen, W.M., Zheng, Z.Q. and Li, M. (2010), "Multi-mode vortex-induced vibration of slender cable experiencing shear flow", *Procedia Eng*., **4**, 145-152.
Daneshvaran, M.T.S. and Vickery, B.J. (1995), "Dynamic response of a compliant tower in wind and waves", *Proceedings of the 27th Annual Offshore Technology Conference*, Houston, Texas, May.
Diana, G., Fiammenghi, G., Belloli, M. and Rocchi, D. (2013), "Wind tunnel tests and numerical approach for long span bridges: The Messina bridge", *J. Wind Eng. Ind. Aerod*., **122**, 38-49.
Gu, M. (2009), "On wind-rain induced vibration of cables of cable-stayed bridges based on quasi-steady assumption", *J. Wind Eng. Ind. Aerod*., **97**(7-8), 381-391.
Holmes, J.D. (2001), *Wind loading of structures*, CRC Press, Boca Raton, FL, USA.
Jain, A., Jones, N.P. and Scanlan, R.H. (1996), "Coupled flutter and buffeting analysis of long-span bridges", *J. Struct. Eng*., ASCE, **122**(7), 716-725.
Jensen, J.J., Olsen, A.S. and Mansour, A.E. (2011), "Extreme wave and wind response predictions", *Ocean Eng*., **38**(17-18), 2244-2253.
Jonkman, J.M. (2007), "Dynamics modelling and load analysis of an offshore floating wind turbine", Technical Report NREL/TP-500-41958, National Renewable Energy Laboratory, University of Colorado.
Kareem, A. (1983), "Nonlinear dynamic analysis of compliant offshore platforms subjected to fluctuating wind", *J. Wind Eng. Ind. Aerod*., **14**(1), 345-356.
Larose, G.L., Falco, M. and Cigada, A. (1995), "Aeroelastic Response of the Towers for the Proposed Bridge over Stretto-Di-Messina", *J. Wind Eng. Ind. Aerod*., **57**(2-3), 363-373.
Larose, G.L., Zasso, A., Melelli, S. and Casanova, D. (1998), "Field measurements of the wind-induced response of a 254 m high free-standing bridge pylon", *J. Wind Eng. Ind. Aerod*., **74-76**, 891-902.
Manenti, S. and Petrini, F. (2010), "Dynamic analysis of an offshore wind turbine: wind-waves nonlinear interaction", *Proceedings of the 12th Biennial International Conference on Engineering, Construction, and Operations in Challenging Environments, ASCE*, Honolulu, Hawaii, March.
McCormick, M.E. (2009), *Ocean Engineering Mechanics: With Applications*, Cambridge University Press, New York, NY, USA.
Philippe, M., Babarit, A. and Ferrant, P. (2013), "Modes of response of an offshore wind turbine with directional wind and waves", *Renew. Energy*, **49**, 151-155.
Ricciardelli, F. (1996), "Prediction of the response of suspension and cable-stayed bridge towers to wind loading", *J. Wind Eng. Ind. Aerod*., **64**(2-3), 145-159.
Siringoringo, D.M. and Fujino, Y. (2012), "Observed along-wind vibration of a suspension bridge tower", *J. Wind Eng. Ind. Aerod*., **103**, 107-121.
Sumer, B.M. and Fredsøe, J. (1997), *Hydrodynamics around cylindrical structures*, World Scientific, Singapore.
Utsunomiya, T., Yoshida, S., Ookubo, H., Sato, I. and Ishida, S. (2014), "Dynamic analysis of a floating offshore wind turbine under extreme environmental conditions", *J. Offshore Mech. Arct. Eng. Trans*., ASME, **136**(2), 020904-1.
Vickery, P. (1995), "Wind-induced response of tension leg platform: theory and experiment", *J. Struct. Eng*., **121**(4), 651-663.
Watanabe, E., Maruyama, T., Tanaka, H. and Takeda, S. (2000), "Design and construction of a floating swing bridge in Osaka", *Mar. Struct*., **13**, 437-458.
Xu, Y.L. and Wang, L.Y. (2003), "Analytical study of wind-rain-induced cable vibration: SDOF model", *J. Wind Eng. Ind. Aerod*., **91**(1-2), 27-40.
Zaheer, M.M. and Islam, N. (2008). "Fluctuating wind induced response of double hinged articulated loading platform", *The 27th International Conference on Offshore Mechanics and Arctic Engineering-ASME*, Estoril, Portugal, June.
Zaheer, M.M. and Islam, N. (2012), "Stochastic response of a double hinged articulated leg platform under wind and waves", *J. Wind Eng. Ind. Aerod*., **111**, 53-60.